Miniature time-of-flight mass analyzer for use in combination with a compact highly-repetitive femtosecond laser ionization source

Yoshinaga, Katsunori
Faculty of Design, Kyushu University

Hao, Nguyen V.
Center of Future Chemistry, Kyushu University

Imasaka, Totaro
Center of Future Chemistry, Kyushu University

Imasaka, Tomoko
Faculty of Design, Kyushu University

出版情報：Analytica Chimica Acta. 1203, pp.339673-, 2022-04-22. Elsevier
バージョン：
権利関係：

Supplementary Information

Miniature time-of-flight mass analyzer for use in combination with a compact highly-repetitive femtosecond laser ionization source

Katsunori Yoshinaga [a], Nguyen V. Hao [b], Totaro Imasaka [b, c, d], and Tomoko Imasaka [a, *]

[a]*Faculty of Design, Kyushu University, 4-9-1, Shiobaru, Minami-ku, Fukuoka 815-8540: 744 Motooka, Nishi-ku, Fukuoka 819-0395, Japan*

[b]*Center of Future Chemistry, Kyushu University,744 Motooka, Nishi-ku, Fukuoka 819-0395, Japan; Present address, Institute of Science and Technology, TNU - University of Sciences, Tan Thinh ward, Thai Nguyen City, Vietnam*

[c]*Kyushu University,744 Motooka, Nishi-ku, Fukuoka 819-0395, Japan*

[d]*Hikari Giken, Co., 2-10-30, Sakurazaka, Chuou-ku, Fukuoka 810-0024, Japan*

* Corresponding author.

Email address: imasaka@design.kyushu-u.ac.jp (Tomoko Imasaka).

Table of contents:

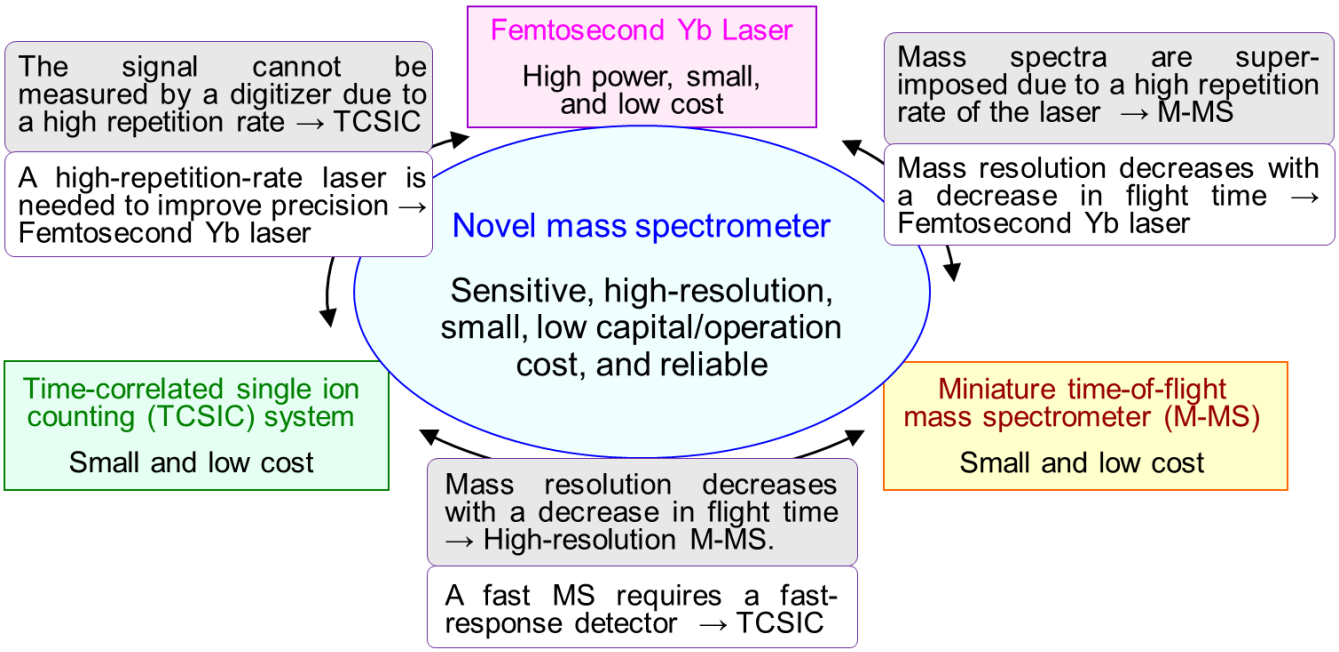

Figure S1. Advantage of using a combination of a highly-repetitive femtosecond Yb laser, a time-correlated single ion counting (TCSIC) system, and a miniature time-of-flight mass spectrometer (M-MS).

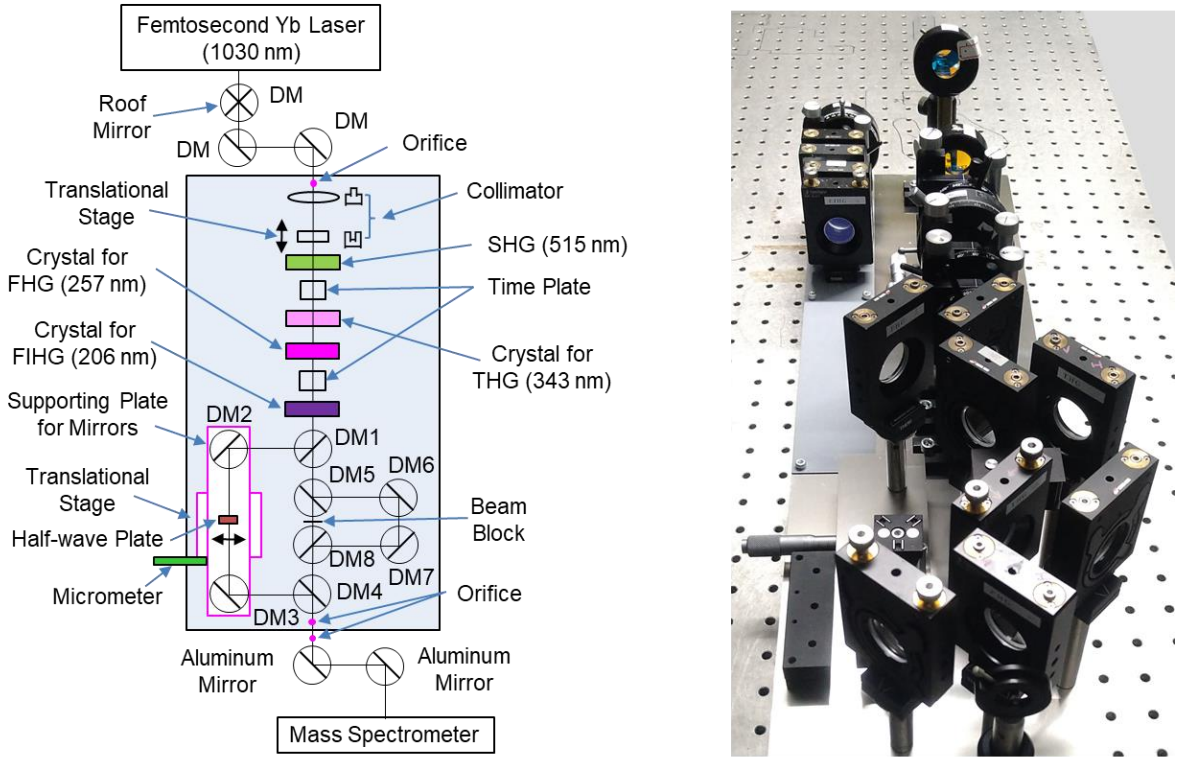

Figure S2. (A) Optical configuration used for the generation of the fifth/third harmonic emissions (B) Photograph of the harmonic generation system.

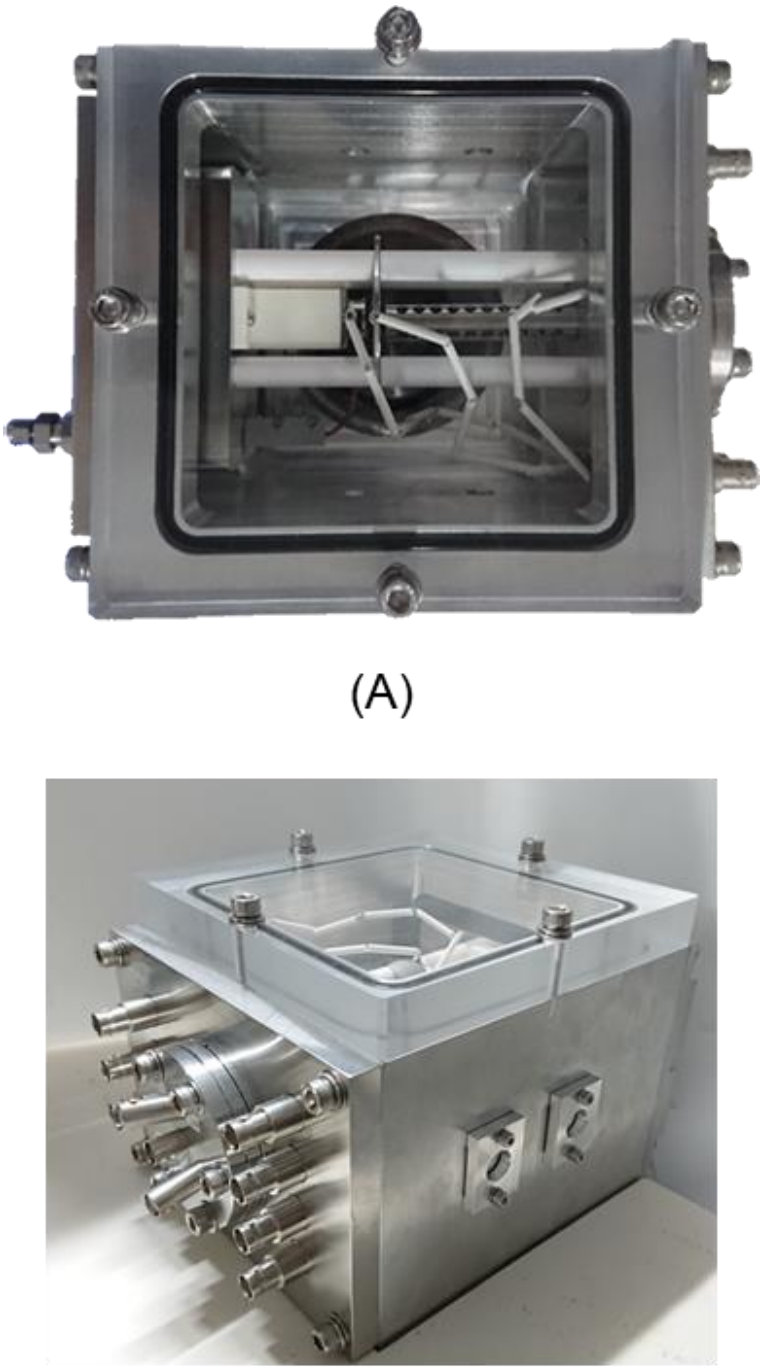

Figure S3. Photograph of a miniature TOFMS. (A) top view (B) right diagonal view.

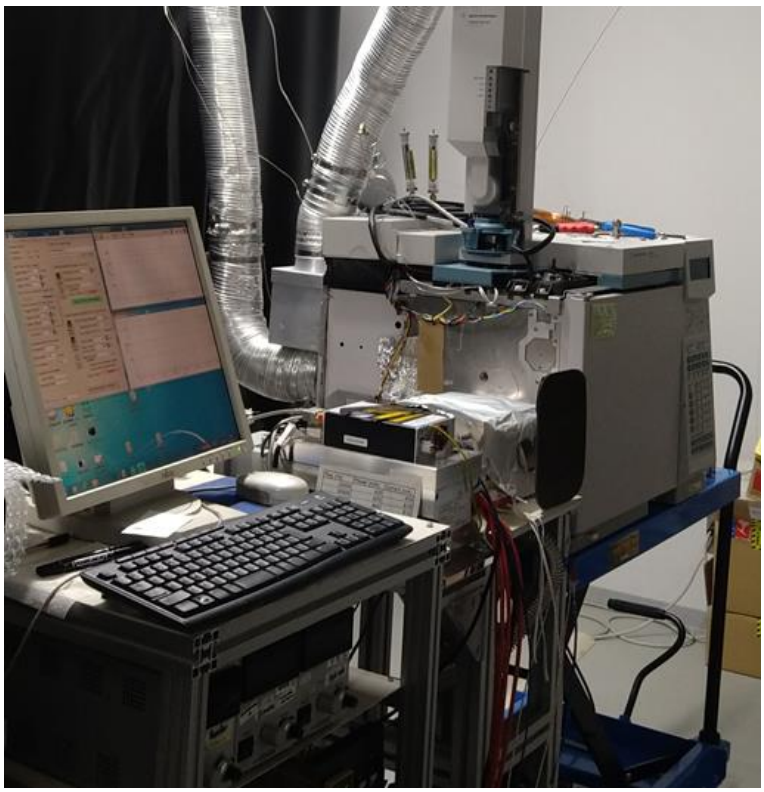

Figure S4. Photograph of the analytical system used for GC-MS. The mass analyzer is located between the GC and the electronics/computer.

Figure S5. Photograph of the system used for sampling the gas using a fused-silica capillary from the exit port of the standard gas generator.

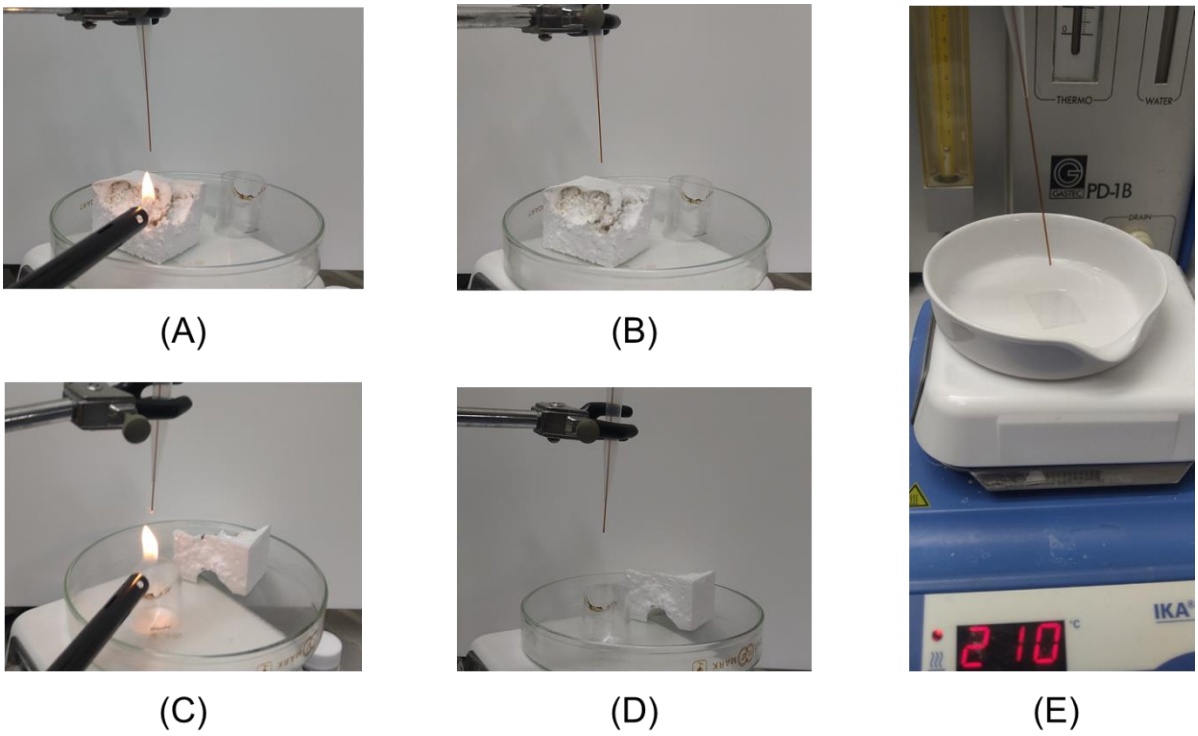

Figure S6. Photographs of scenes showing (A) (C) burning and (B) (D) sampling the combustion products of (A) (B) polystyrene foam and (C) (D) polycarbonate film, and (E) vaparizing a liquid sample such as DIMP and DMMP in an evaporating dish rapidly heated on a hot plate to vaporize in the air.

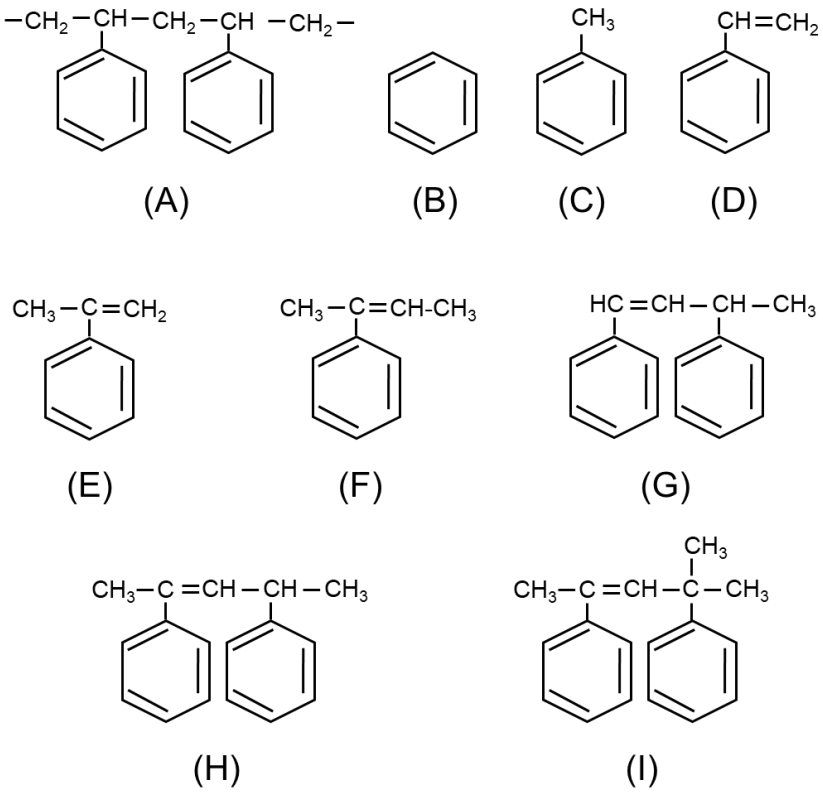

Figure S7. Chemical structures of the combustion products suggested from the data of thermally decomposed products of polystyrene (see ref. S1).

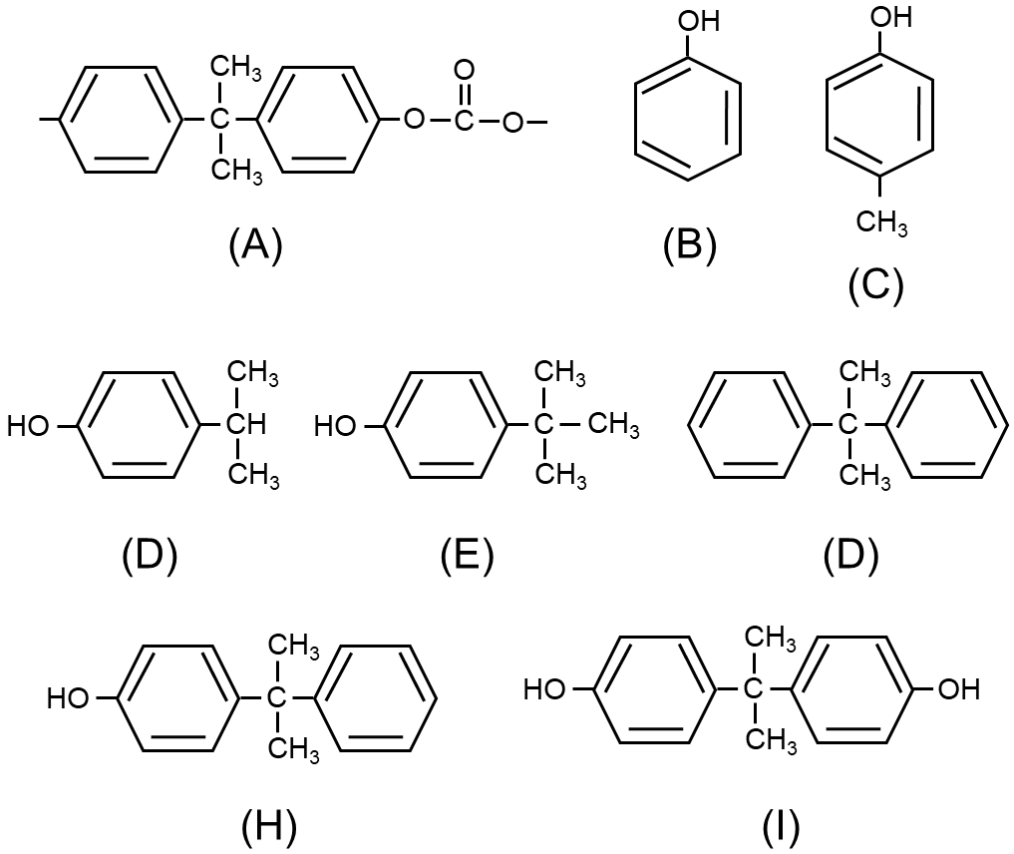

Figure S8. Chemical structures of the combustion products based on the data obtained for thermally decomposed products of polycarbonate (see ref. 1).

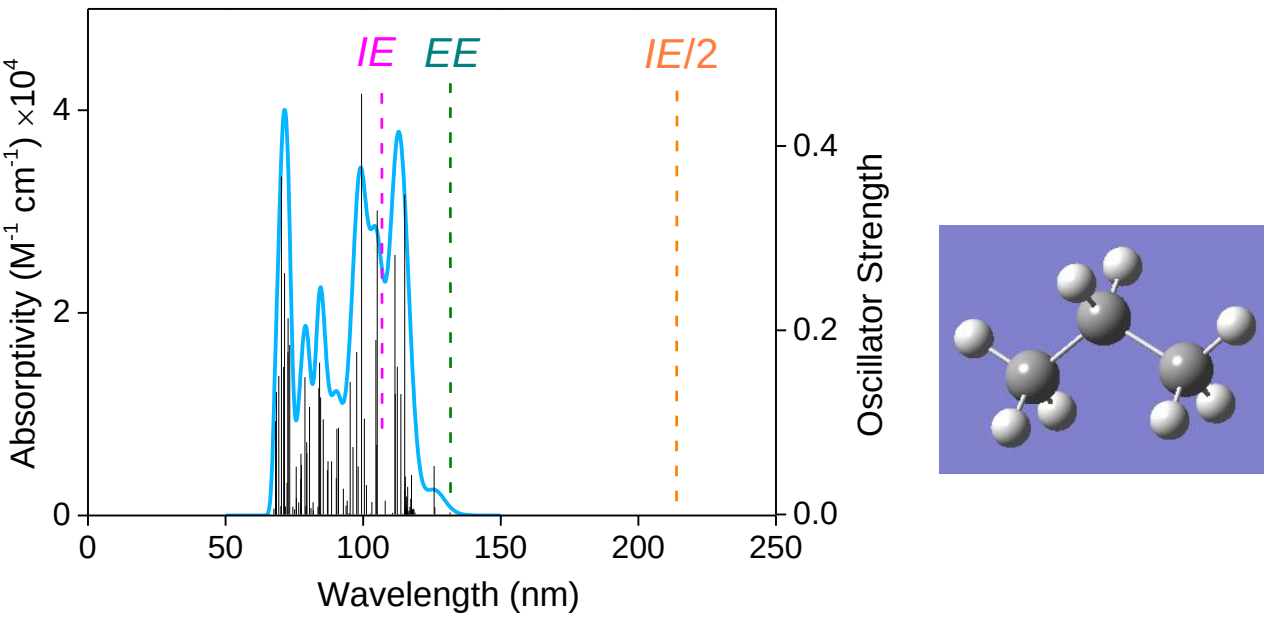

Figure S9. Spectral properties of propane calculated by TD-DFT.

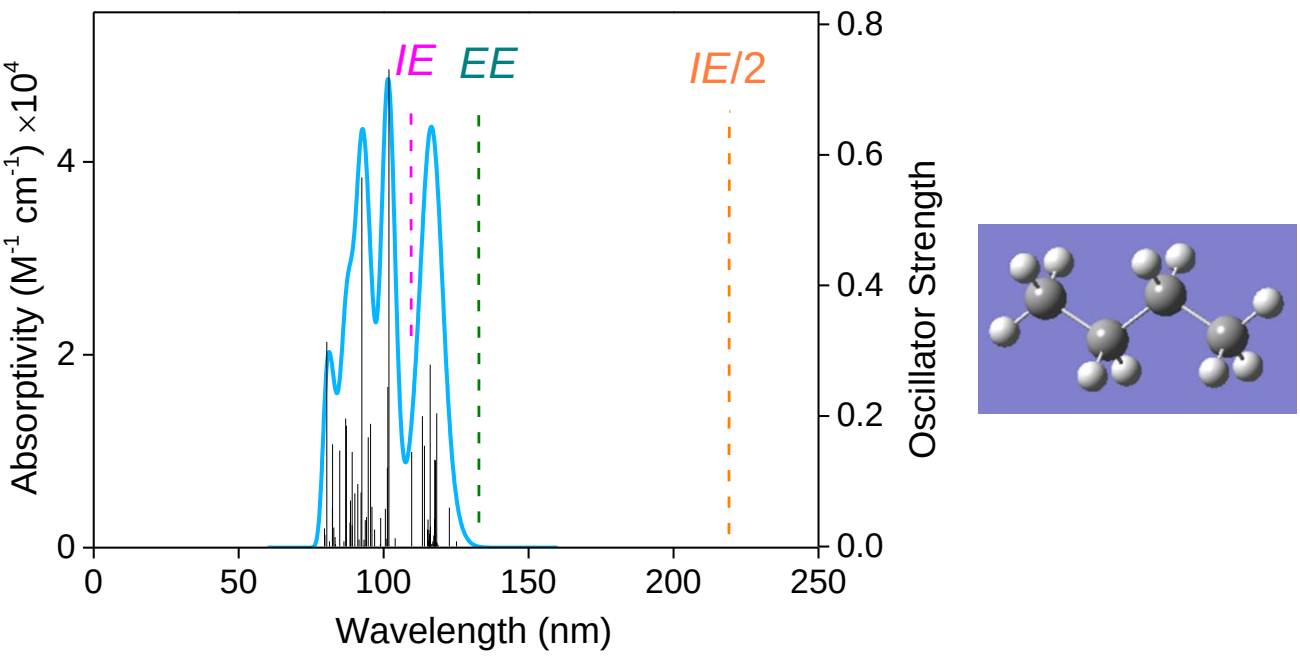

Figure S10. Spectral properties of butane calculated by TD-DFT.

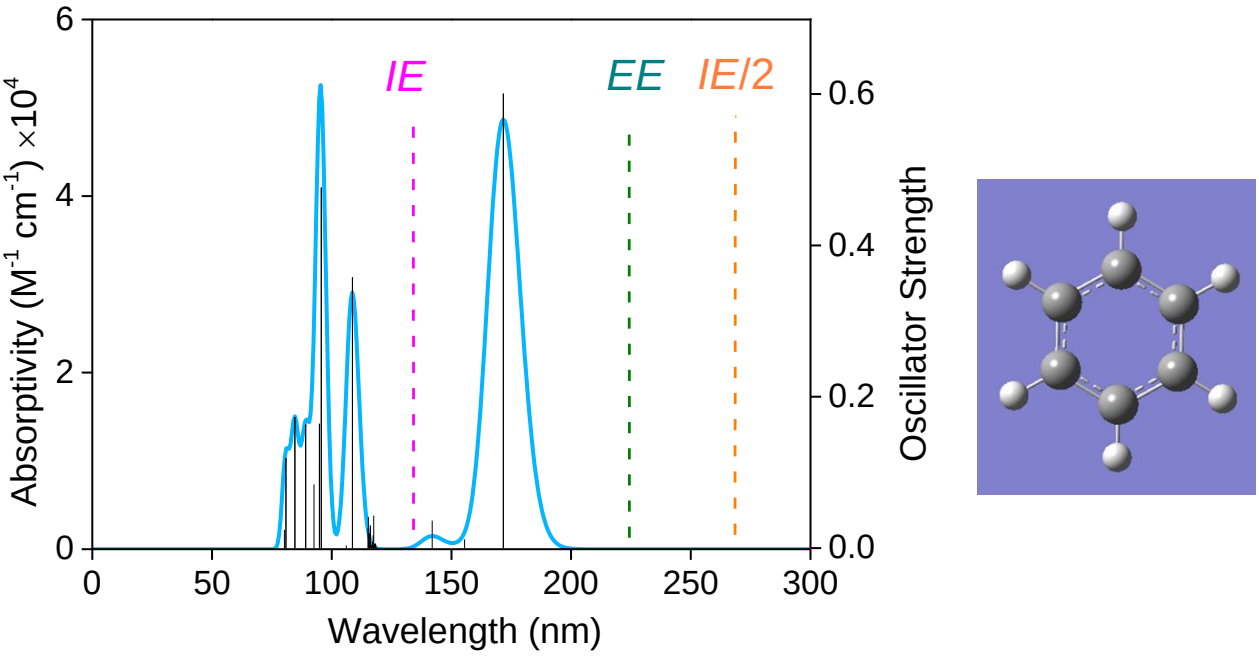

Figure S11. Spectral properties of benzene calculated by TD-DFT.

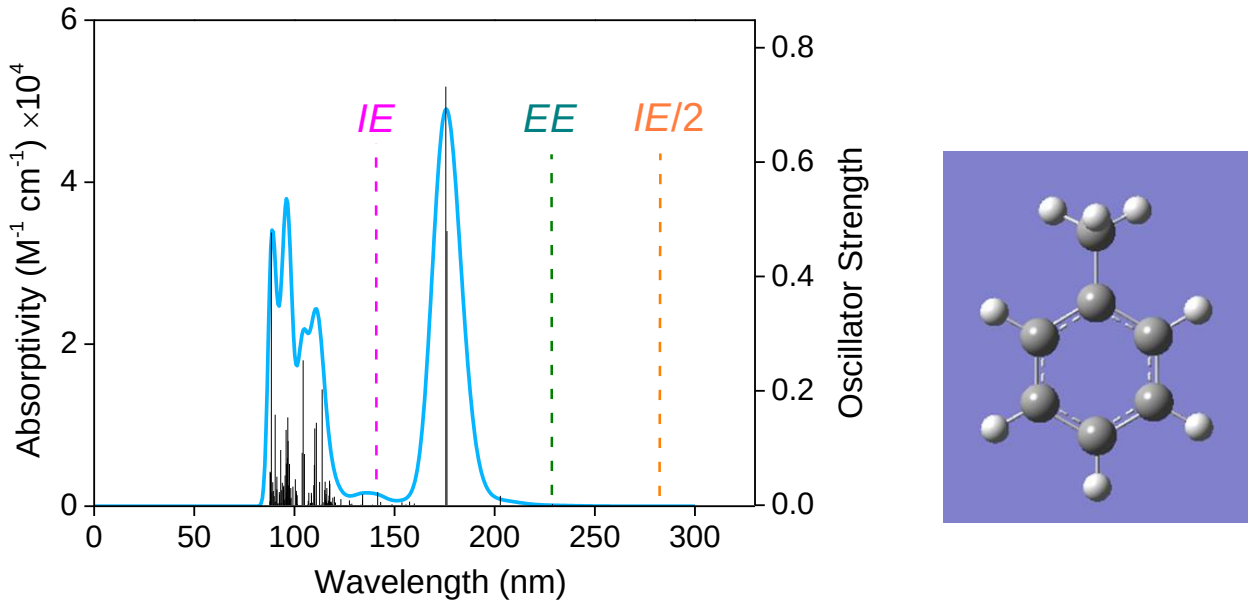

Figure S12. Spectral properties of toluene calculated by TD-DFT.

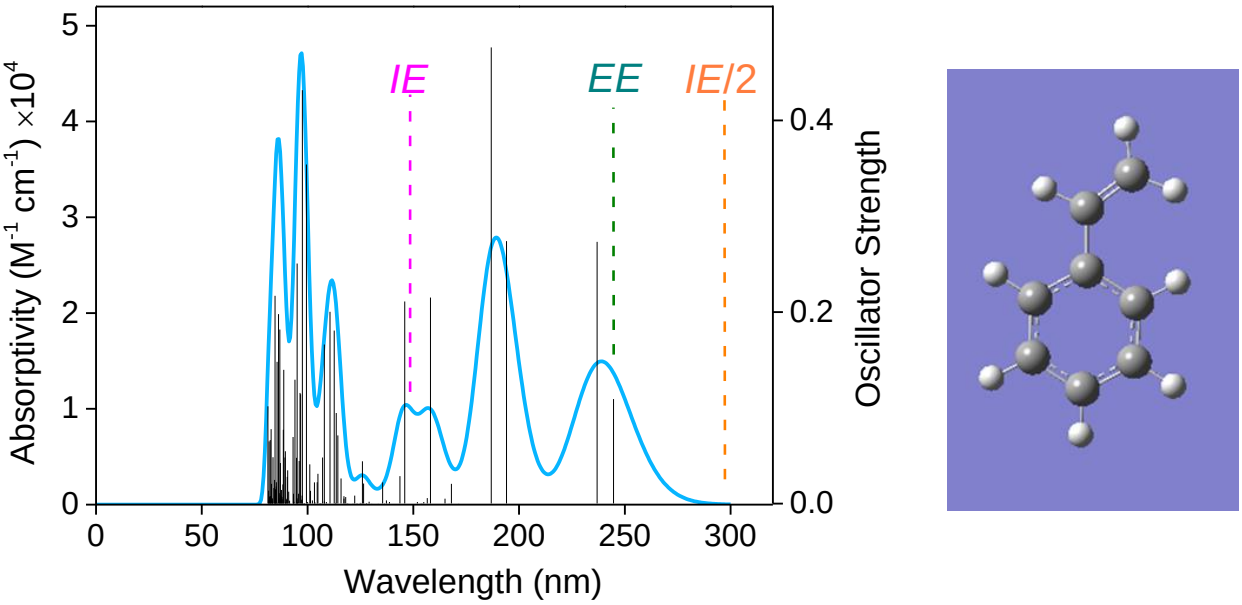

Figure S13. Spectral properties of styrene calculated by TD-DFT.

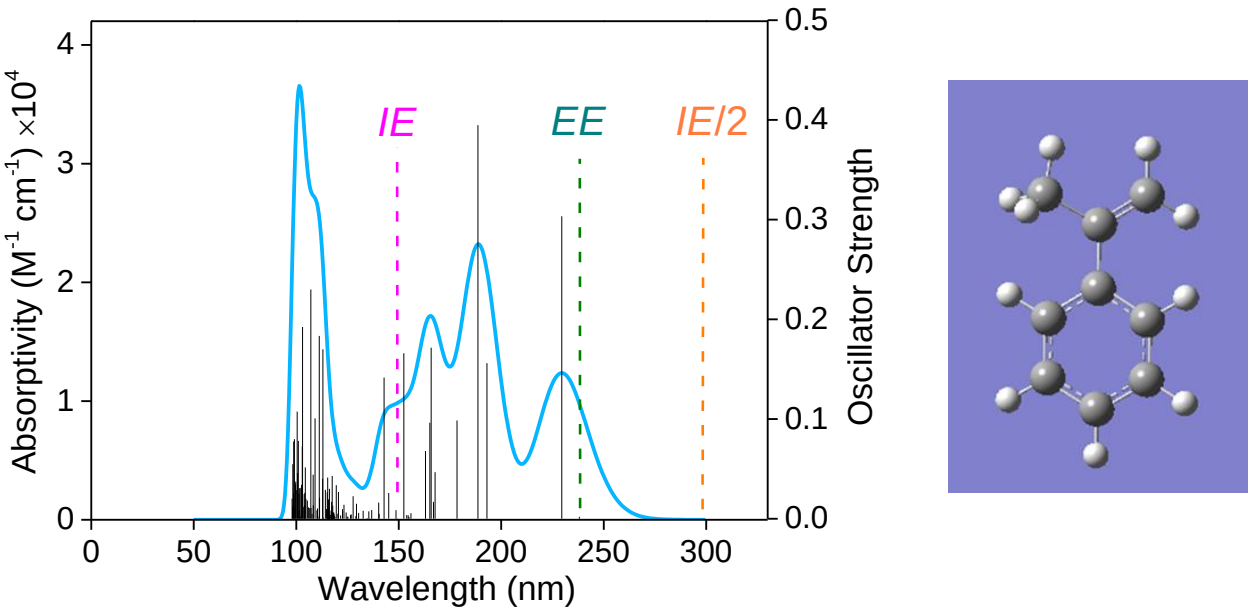

Figure S14. pectral properties of α-methylstyrene calculated by TD-DFT.

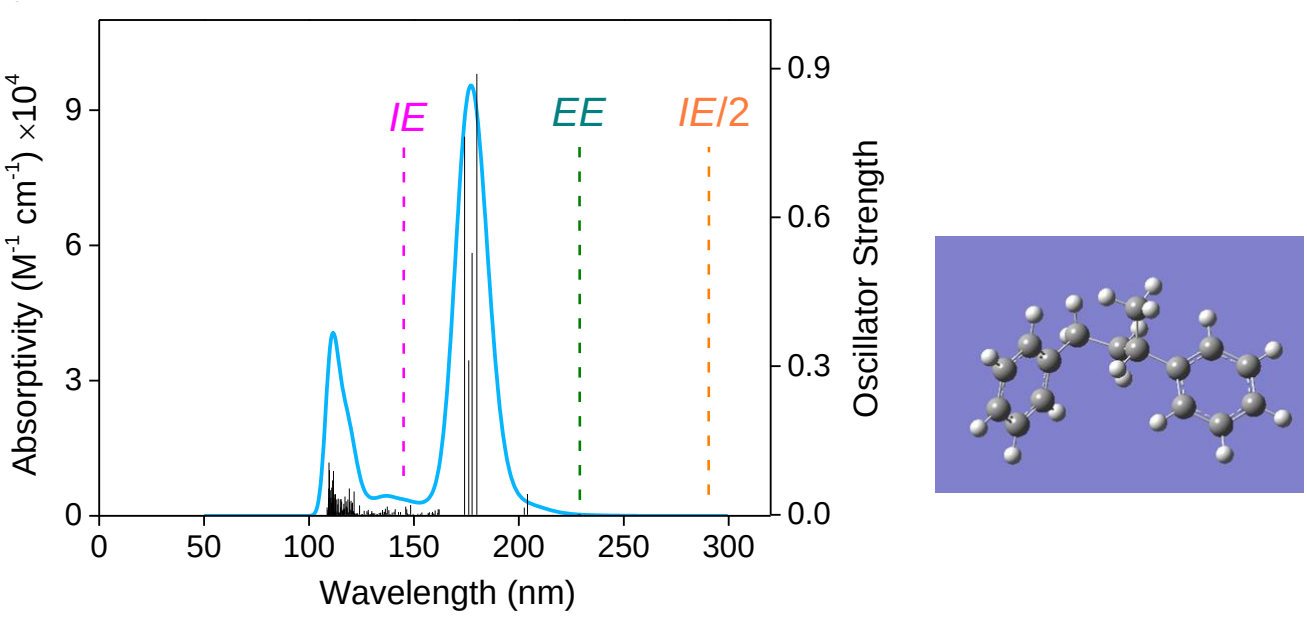

Figure S15. Spectral properties of 1,3-diphenylbutane calculated by TD-DFT.

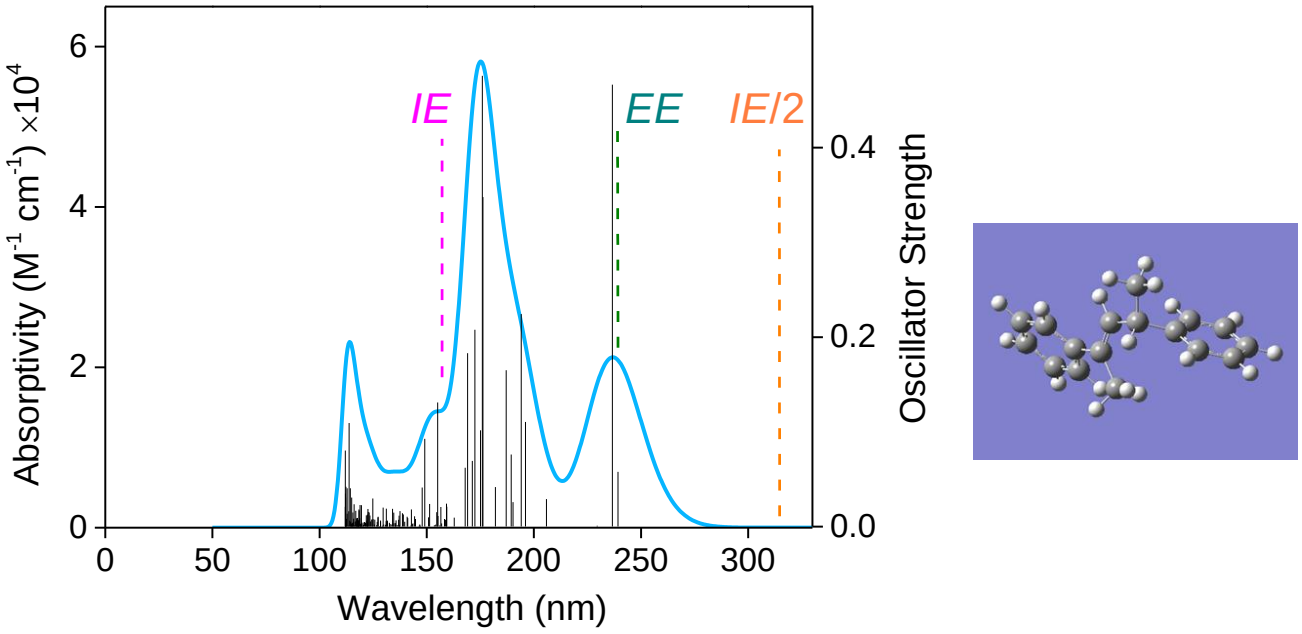

Figure S16. Spectral properties of 2,4-diphenyl-2-pentene calculated by TD-DFT.

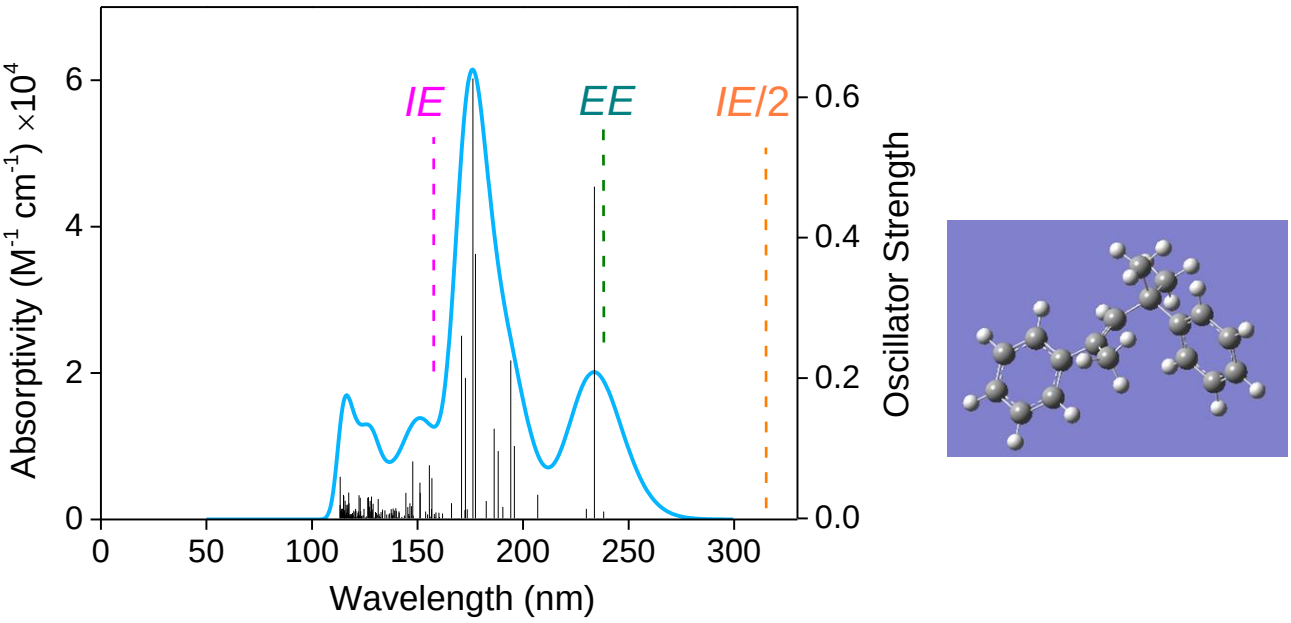

Figure S17. Spectral properties of 2,4-diphenyl-4-methyl-2(E)-pentene calculated by TD-DFT.

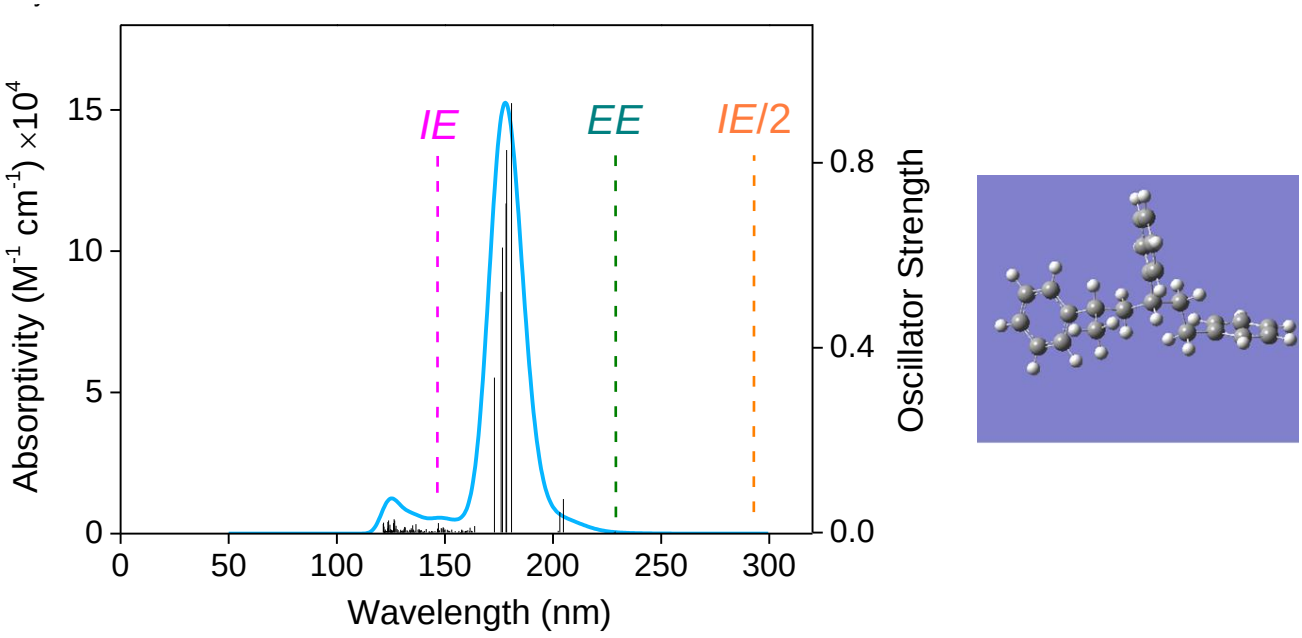

Figure S18. Spectral properties of 1,3,5-triphenylhexane calculated by TD-DFT.

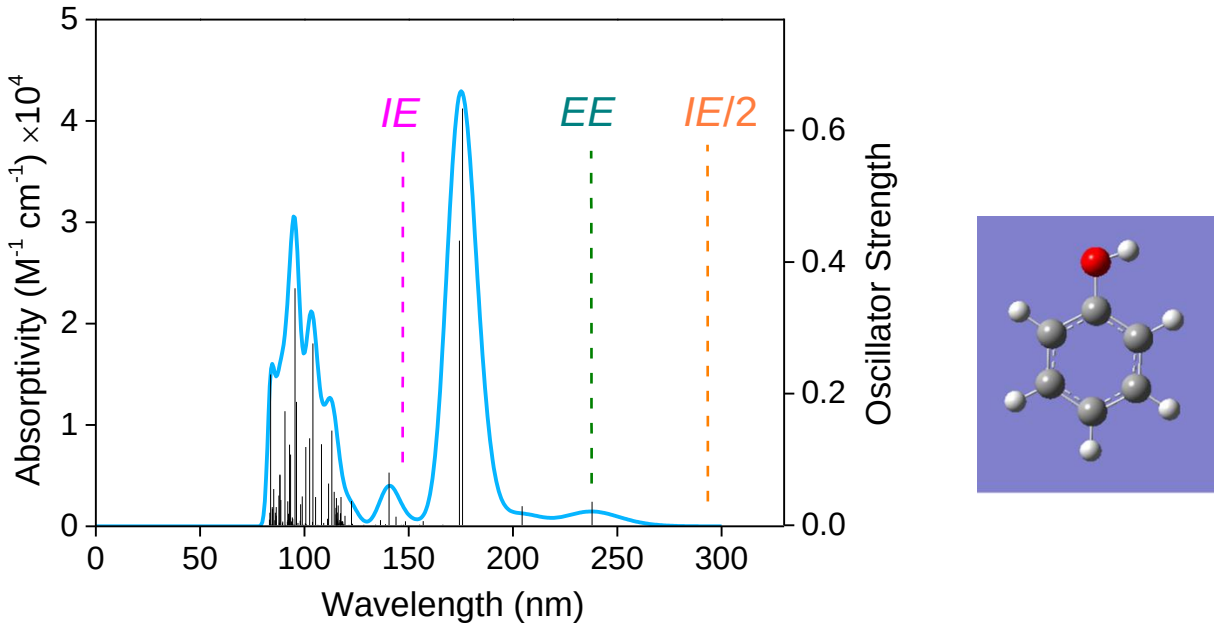

Figure S19. Spectral properties of phenol calculated by TD-DFT.

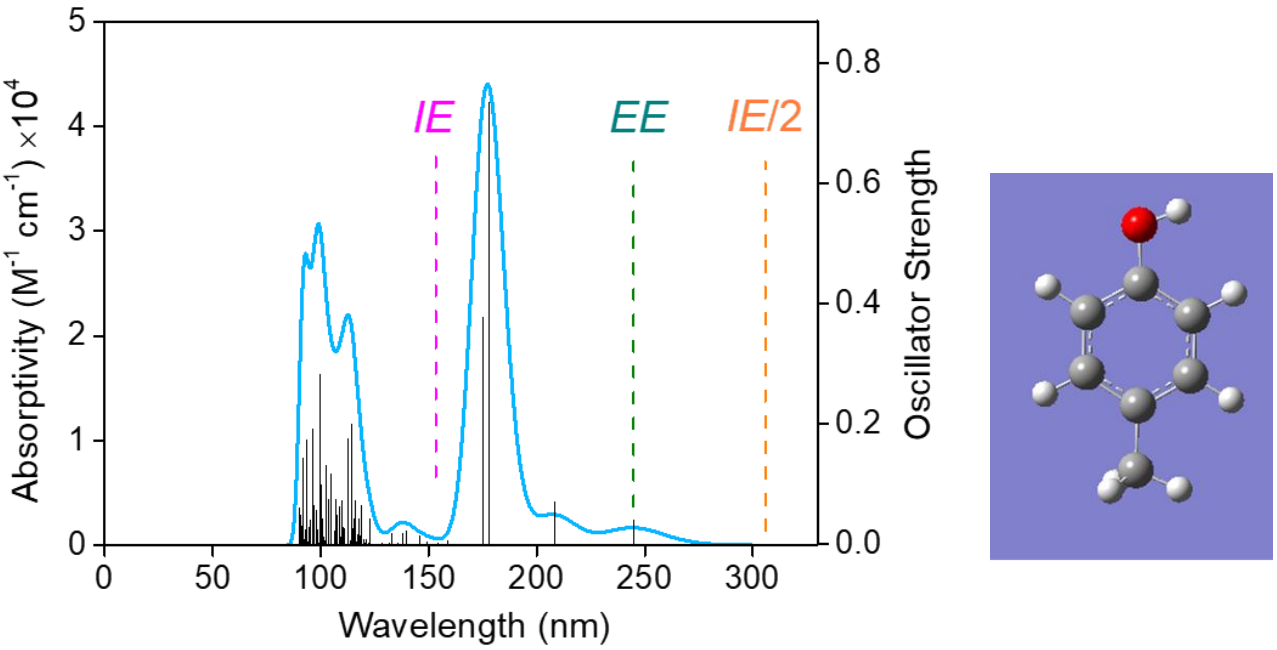

Figure S20. Spectral properties of p-cresol calculated by TD-DFT.

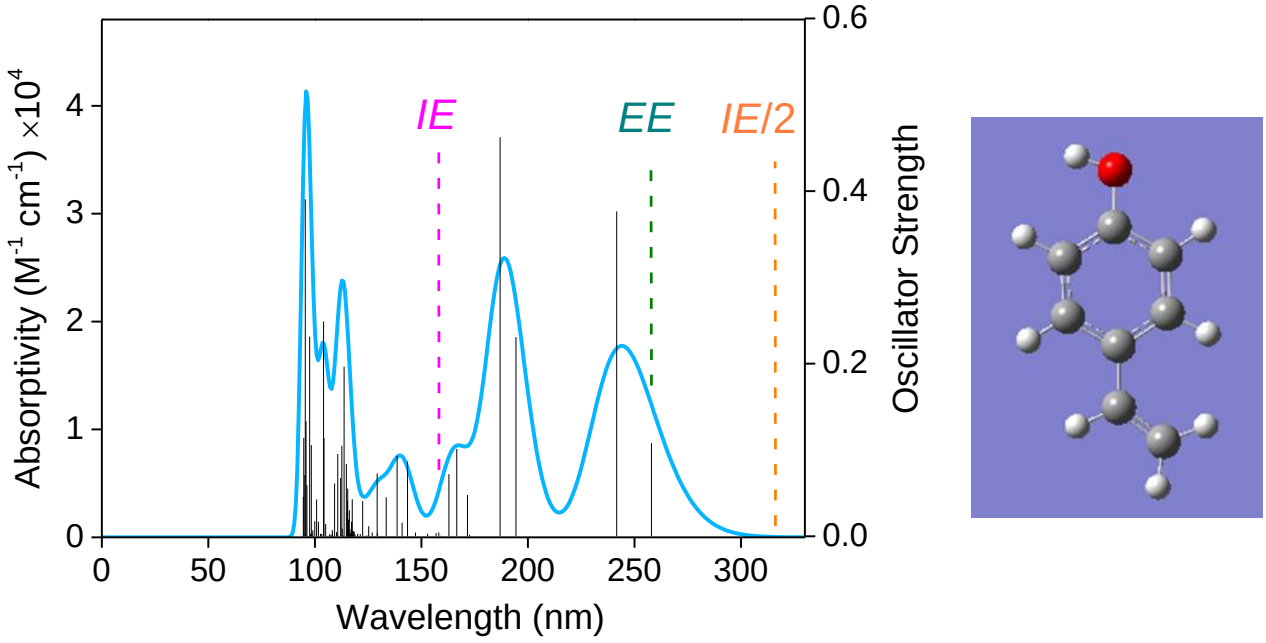

Figure S21. Spectral properties of p-vinylphenol calculated by TD-DFT.

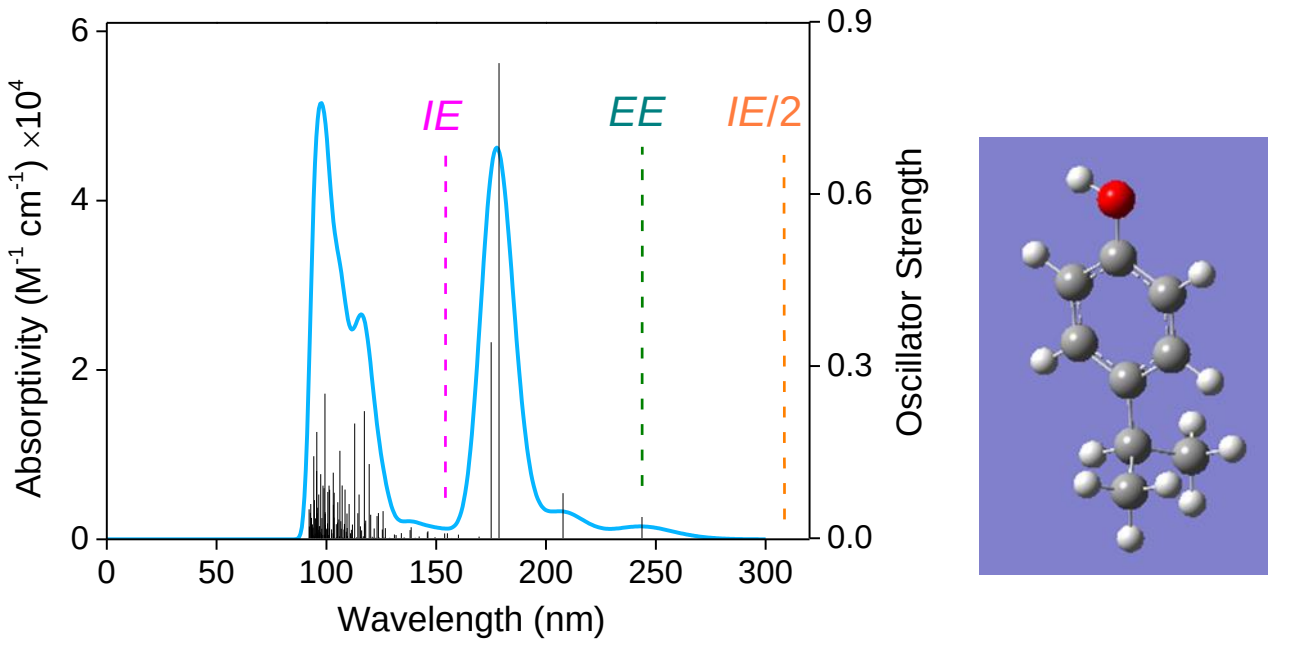

Figure S22. Spectral properties of 4-isopropylphenol calculated by TD-DFT.

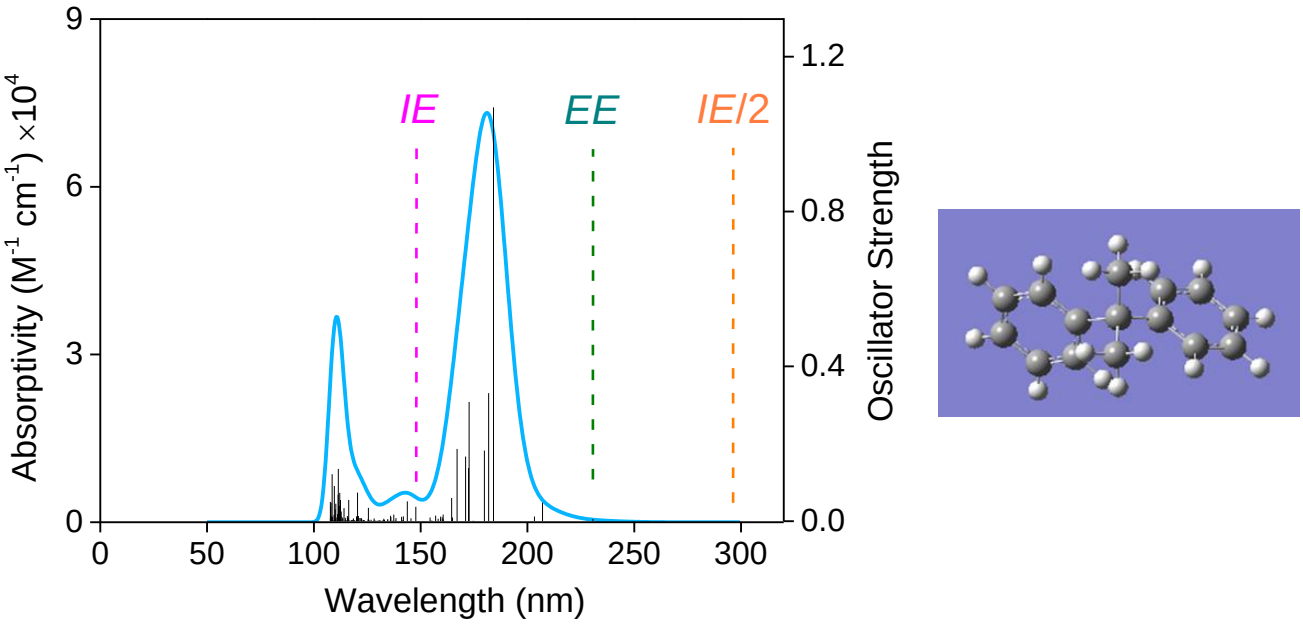

Figure S23. Spectral properties of dimethyldiphenylmethane calculated by TD-DFT.

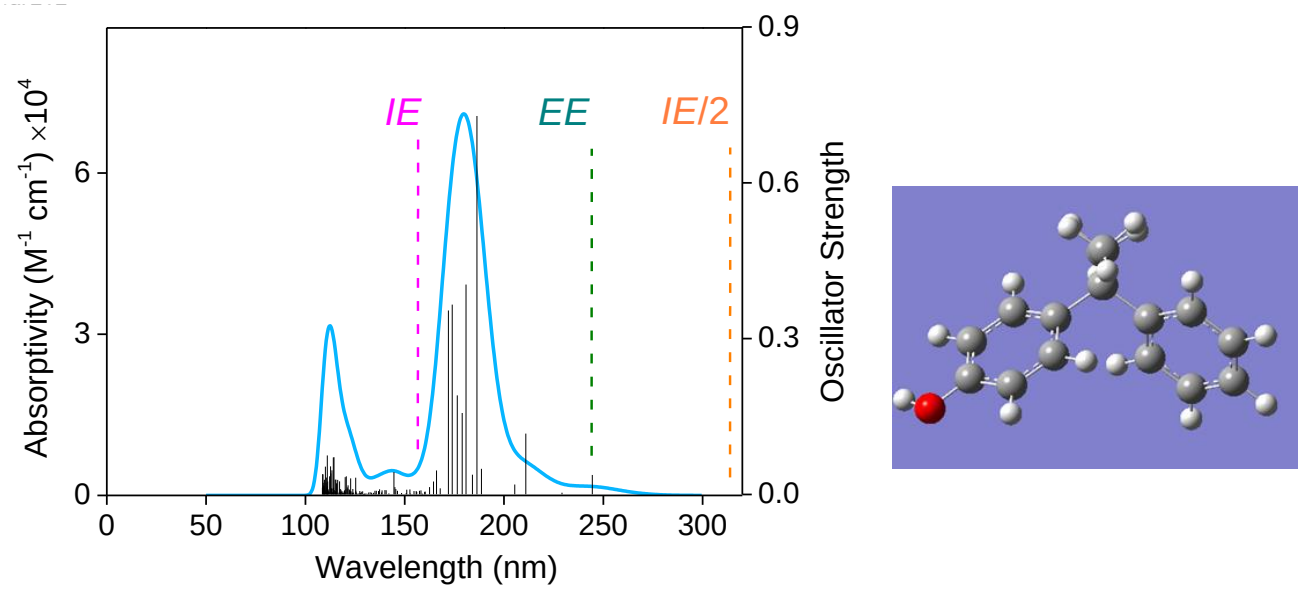

Figure S24. Spectral properties of 4-hydroxydiphyenyldimethylmethane calculated by TD-DFT.

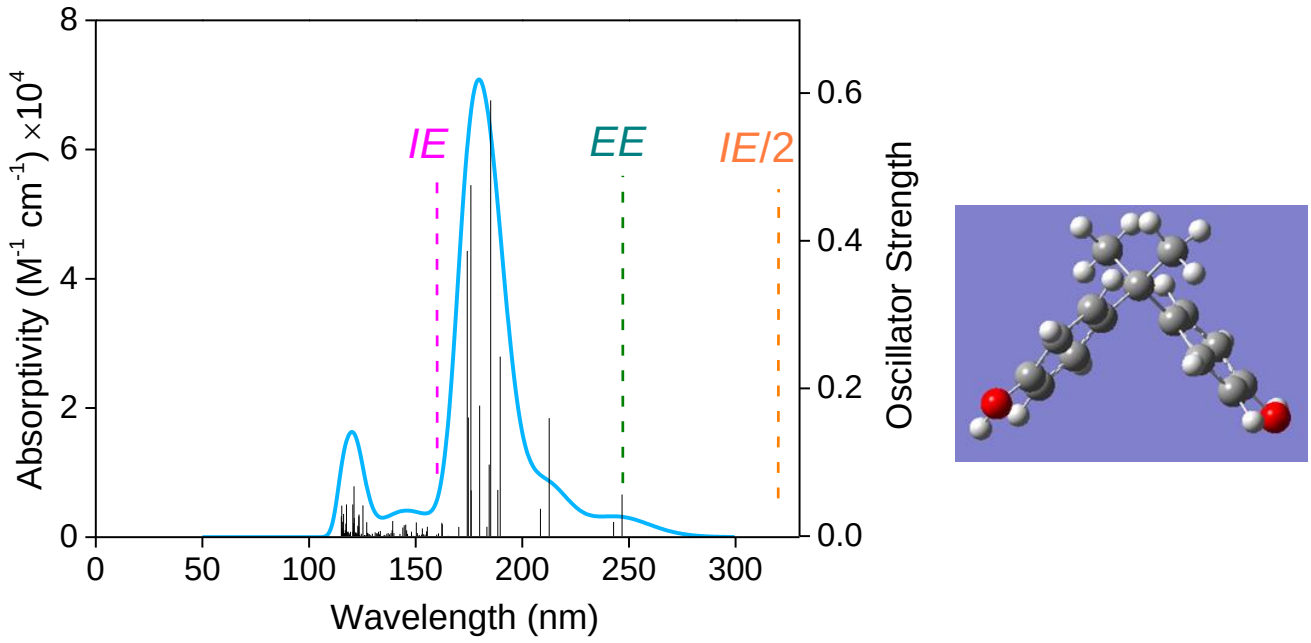

Figure S25. Spectral properties of bisphenol A calculated by TD-DFT.

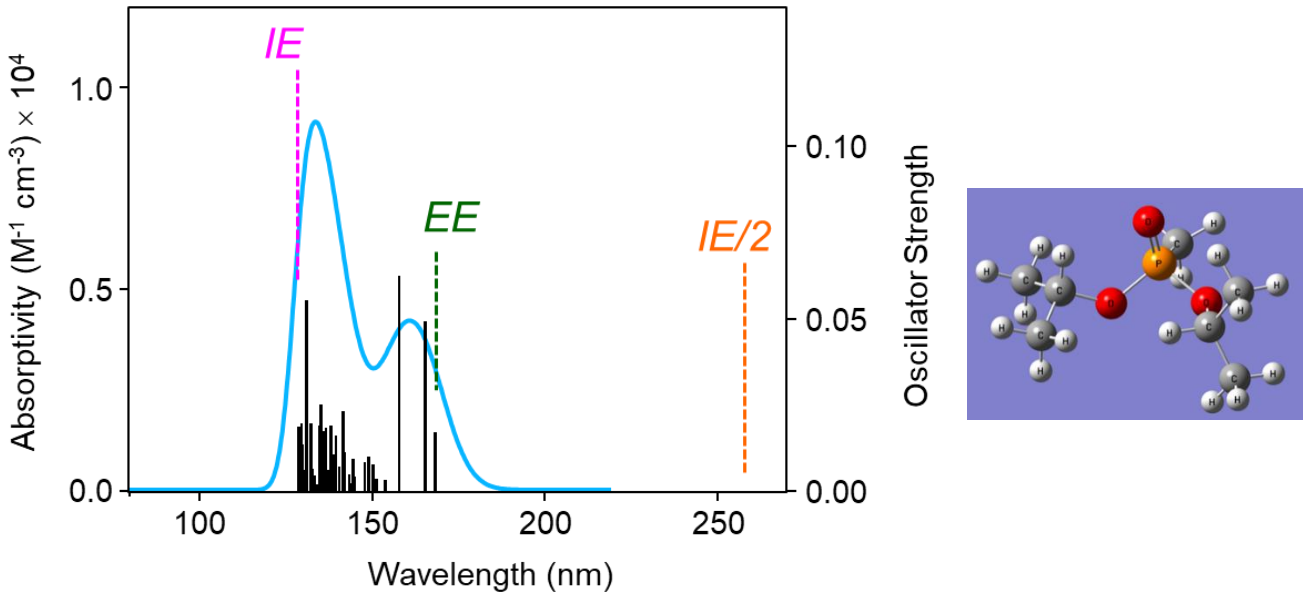

Fig. S26. Spectral properties of DIMP calculated by TD-DFT. *IE*, (1) 9.63 eV or 128.7 nm (B3LYP/cc-pVTZ//B3LYP/cc-pVDZ), (2) 9.93 eV or 124.8 nm (WB97XD/cc-pVTZ//B3LYP/cc-pVDZ) (3) no data available in NIST.

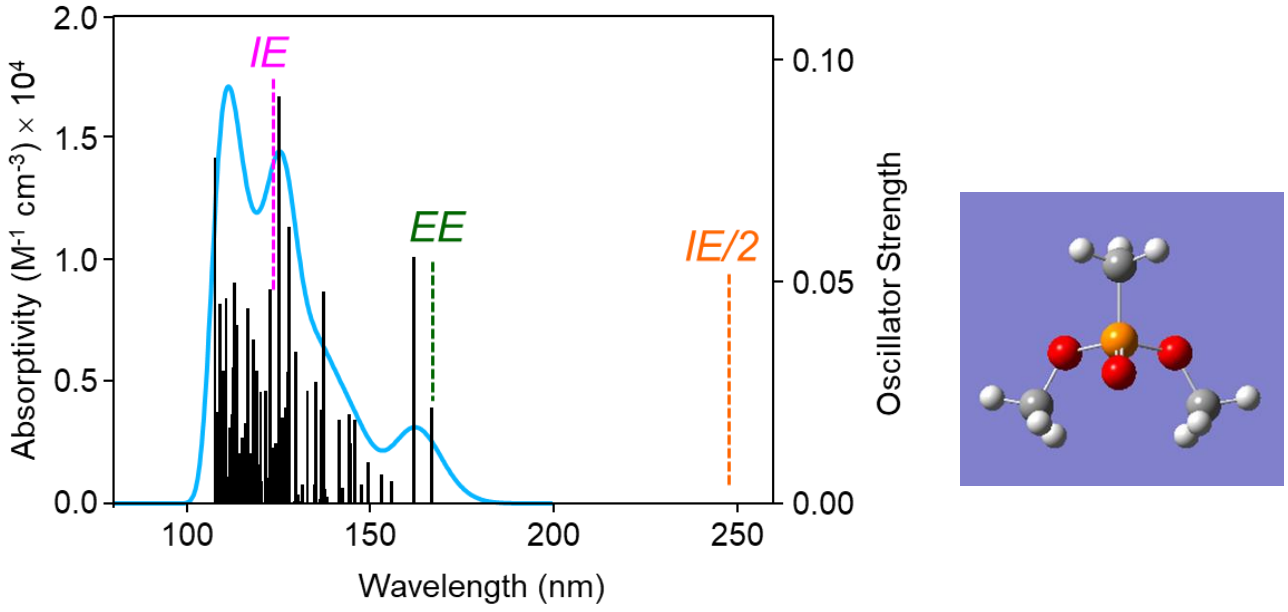

Fig. S27. Spectral properties of DMMP calculated by TD-DFT. *IE*, (1) 10.03 eV or 123.7 nm (B3LYP/cc-pVTZ//B3LYP/cc-pVDZ) (2) 10.30 eV or 120.4 nm (WB97XD/cc-pVTZ//B3LYP/cc-pVDZ) (3) 10.00 eV or 124.0 nm in NIST.

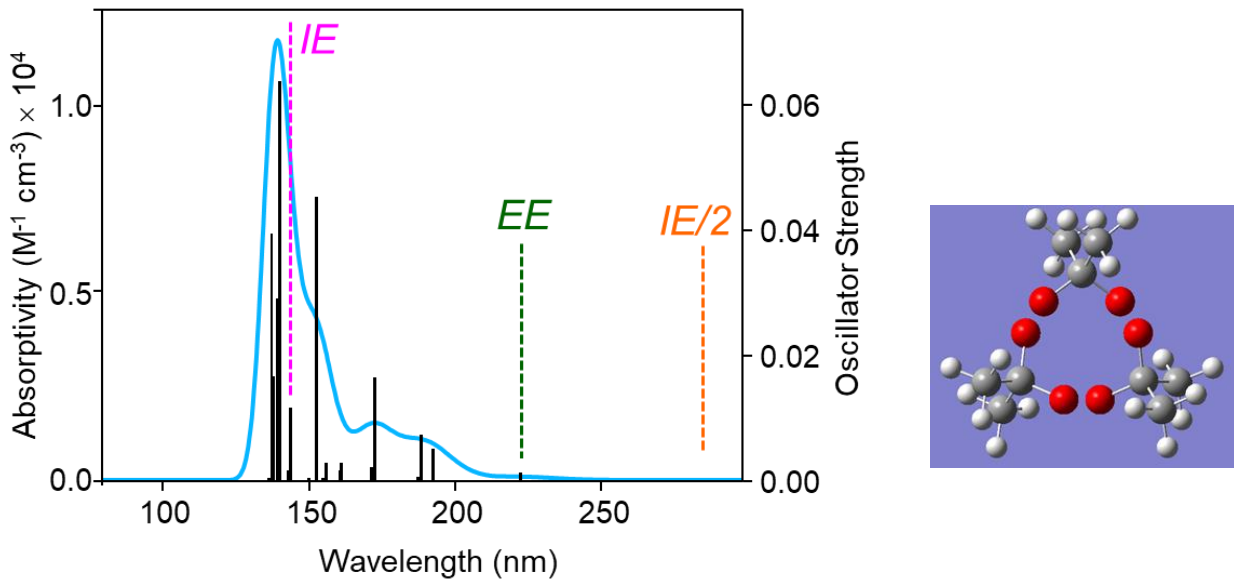

Fig. S28. Spectral properties of TATP calculated by TD-DFT. *IE*, 8.67 eV or 142.94 nm; *EE*, 5.53 eV or 224.01 nm.

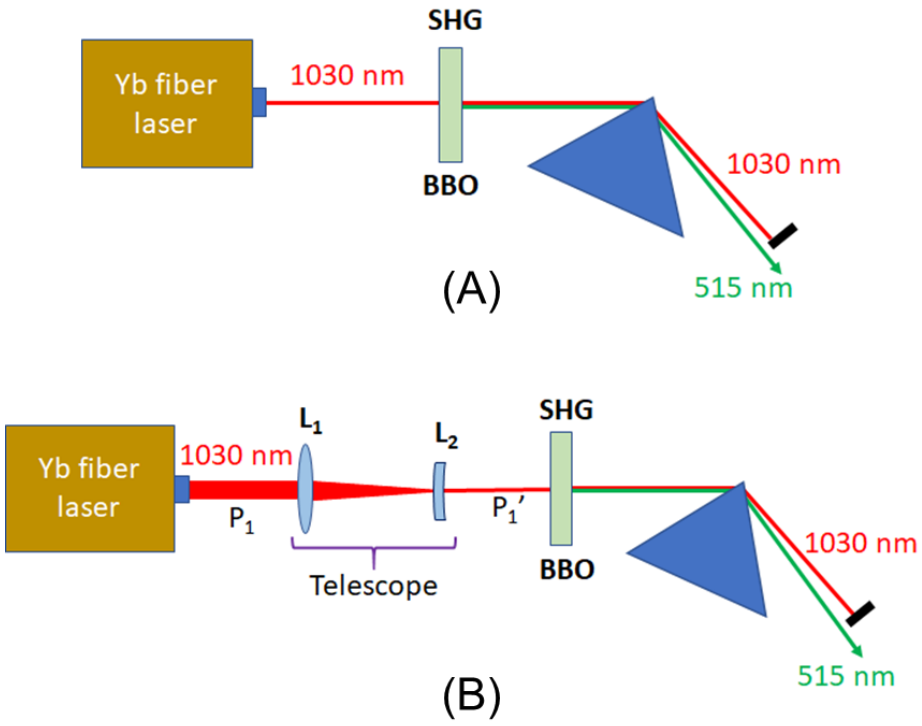

Figure S29. Block diagram showing the generation and measurement of the second harmonic emission of the Yb laser. (A) no telescope (B) with telescope (200 mm, -50 mm, anti-reflection coating). Laser power, 2.46 W; wavelength,1032 nm; repetition rate, 120 kHz; beam diameter. 3 mm; beam propagation factor, M^2 < 1.2; beam polarization, p-polarized; pulse energy, 20.4 μJ. (A) peak intensity at the BBO crystal, I = 1.44 GW/cm^2; output power of the second harmonic emission, 210 mW; conversion efficiency, 8.6 %. (B) beam diameter, 0.75 mm; I = 23 GW/cm^2; output power of the second harmonic emission, 930 mW: reflective loss on a prism, 205 mW (9.15 %). The output power of the second harmonic emission generated by a BBO crystal was 1010 mW (conversion efficiency, 41.1 %). The spectral bandwidth of the second harmonic beam was 1.9 nm (FWHM).

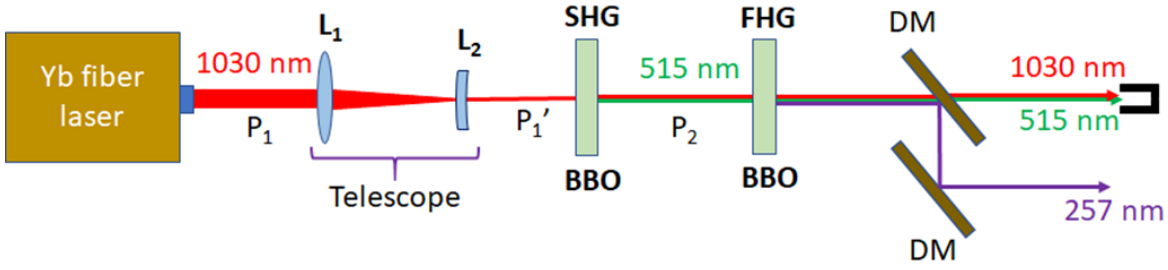

Figure S30. Block diagram showing the generation and measurement of the fourth harmonic emission of the Yb laser. The fourth harmonic beam was separated from remaining second harmonic and fundamental beams using two dichroic mirrors. The output power achieved for the fourth harmonic beam was 480 mW (conversion efficiency from 1032 nm to 257 nm, 19.7 %). The spectral bandwidth of the fourth harmonic beam was 2.15 nm (FWHM). Note that a conversion efficiency from 1032 nm to 257 nm is reported to be 9.37% (213 fs, 796 kHz, 80 W) in ref. S2.

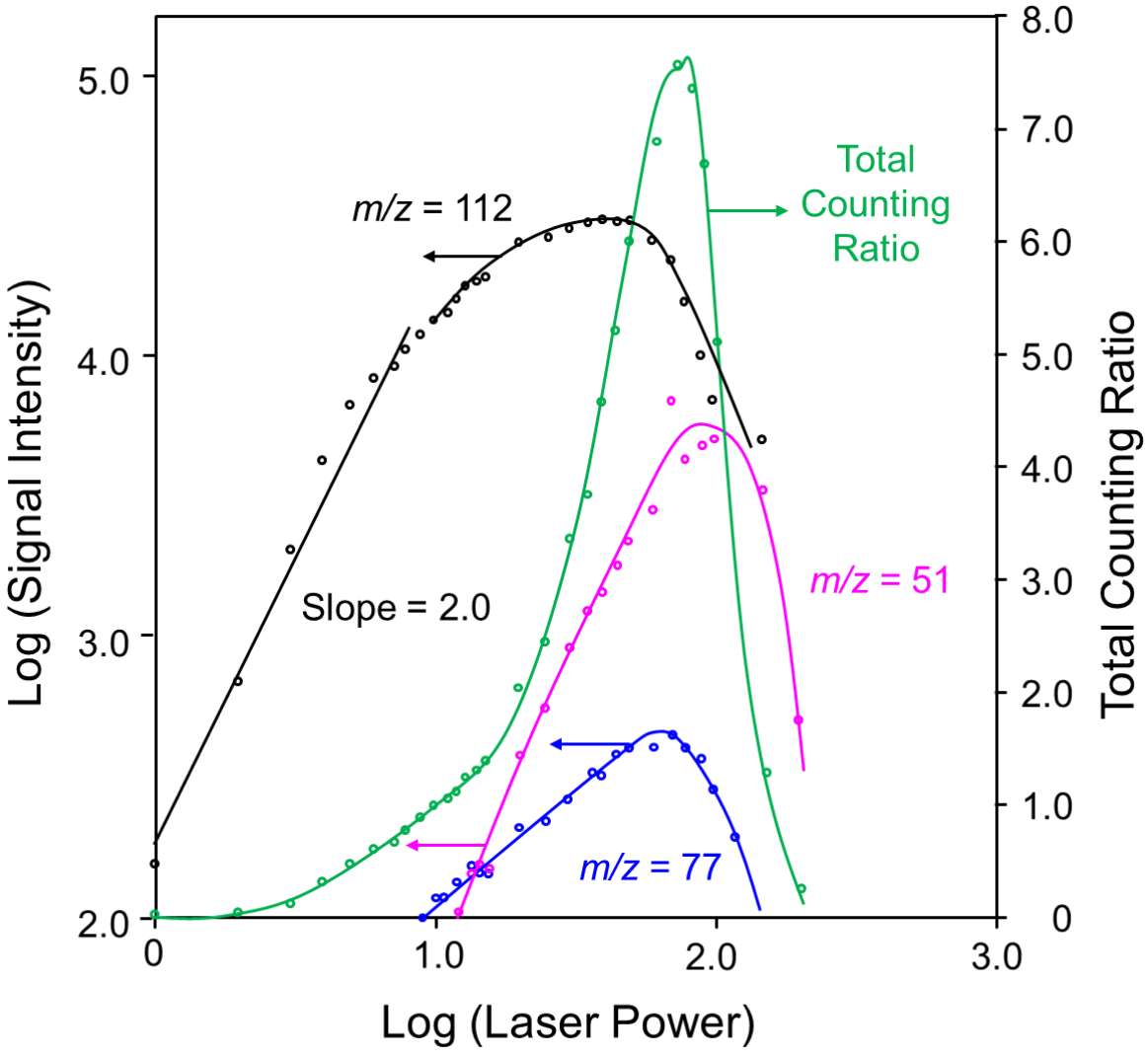

Figure S31. Dependence of the signal intensities of the molecular and fragment ions on the laser pulse energy. Sample, chlorobenzene. The total counting ratio is shown in the right-hand scale.

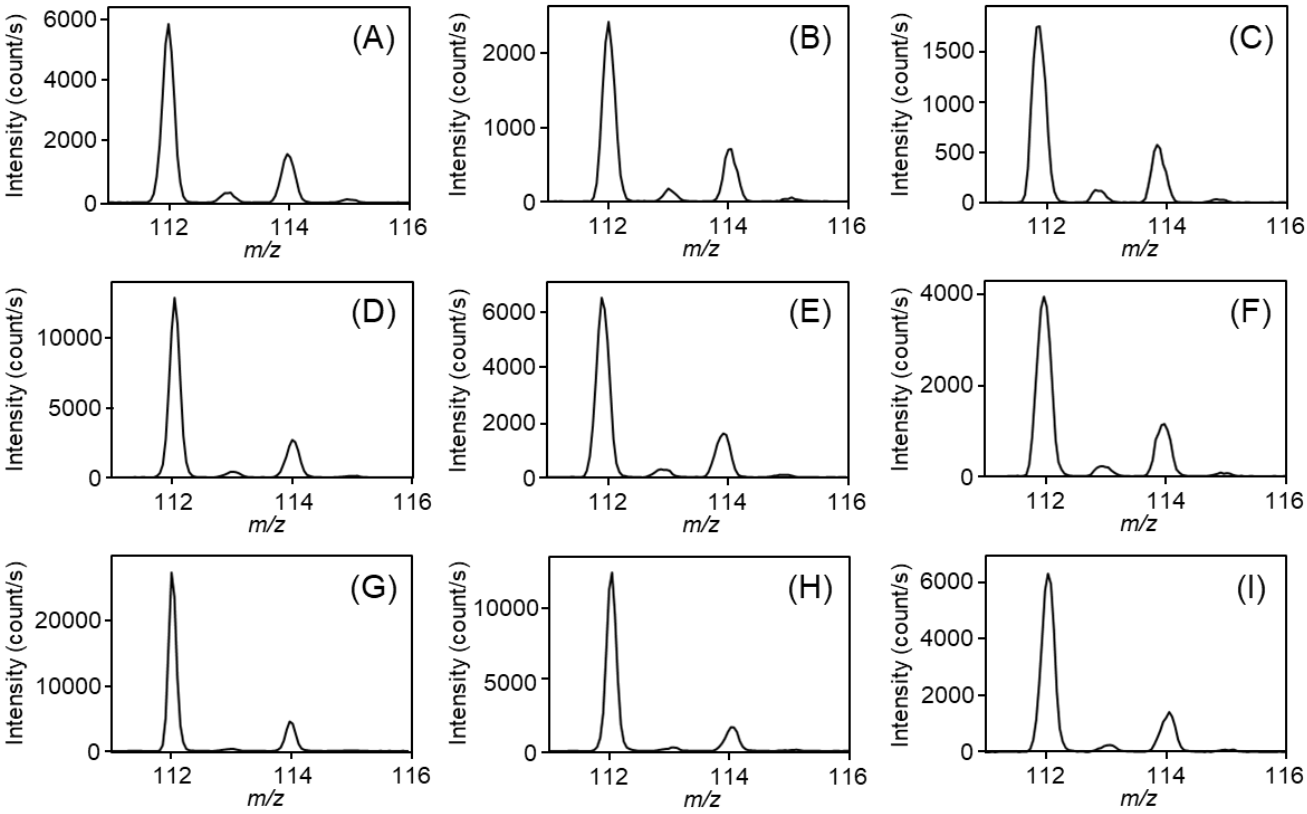

Figure S32. Dependence of the signal intensity of the molecular ion for chlorobenzene on the repetition rate of the Yb laser. Laser power at 257 nm; (A) – (C) 5 mW, (D) – (F) 10 mW, (G) – (I) 20 mW. Repetition of the laser; (A) (D) (G) 120 kHz, (B) (E) (H) 274 kHz, (C) (F) (I) 560 kHz.

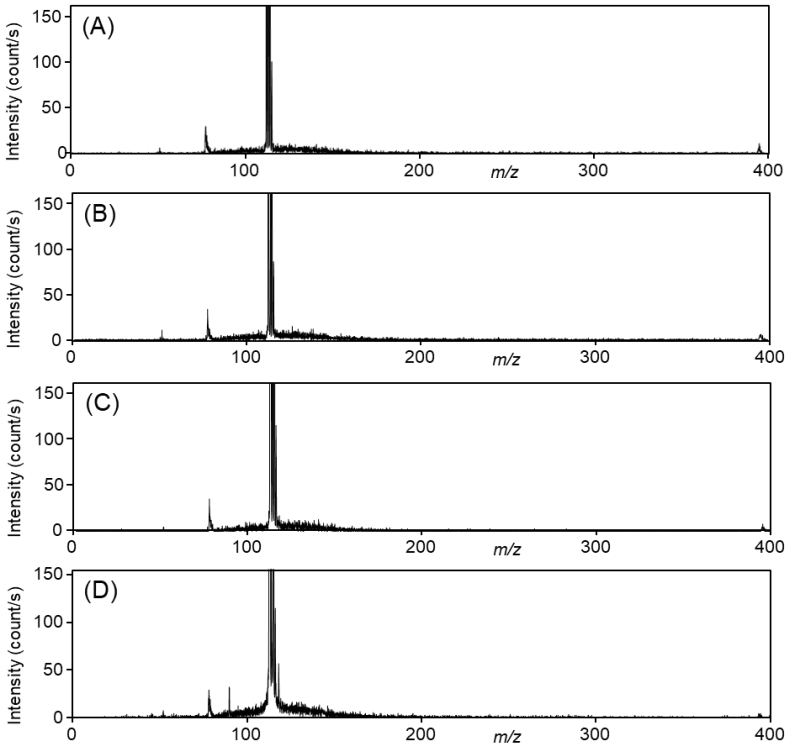

Figure S33. Mass spectra of chlorobenzene measured at different background pressures in the vacuum chamber. (A) 4×10^{-4} Pa (B) 2×10^{-3} Pa (C) 4×10^{-3} Pa (D) 2×10^{-2} Pa. Laser output power, 5 mW.

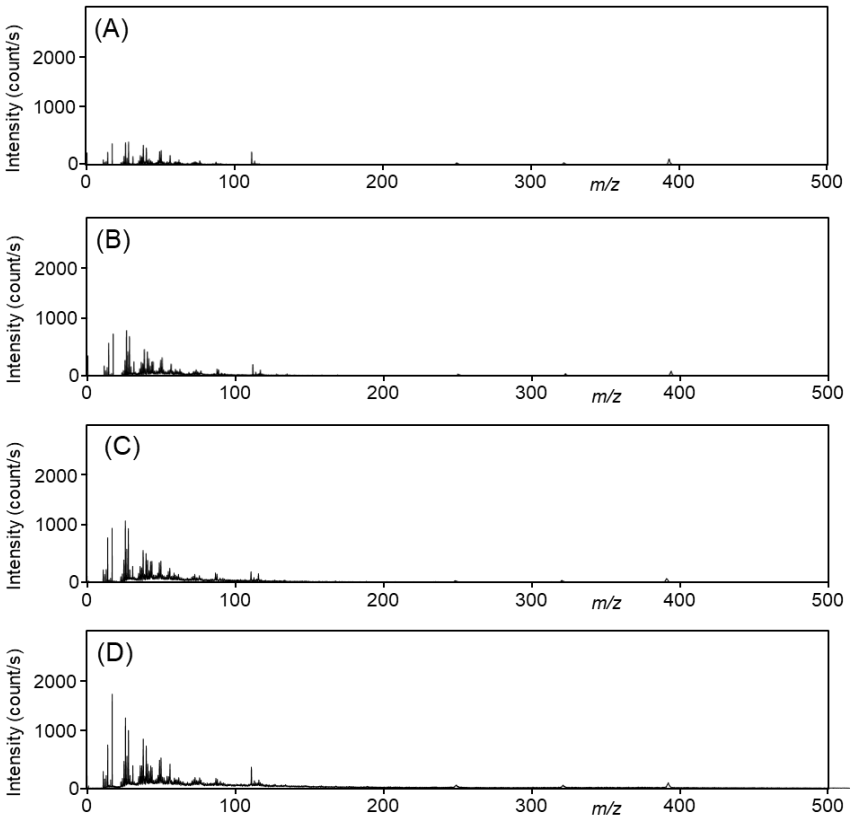

Figure S34. Dependence of the background signal intensity on the background gas pressure in the vacuum chamber. (A) 2×10^{-4} Pa (B) 2×10^{-3} Pa (C) 4×10^{-3} Pa (D) 2×10^{-2} Pa. Laser output power, 250 mW.

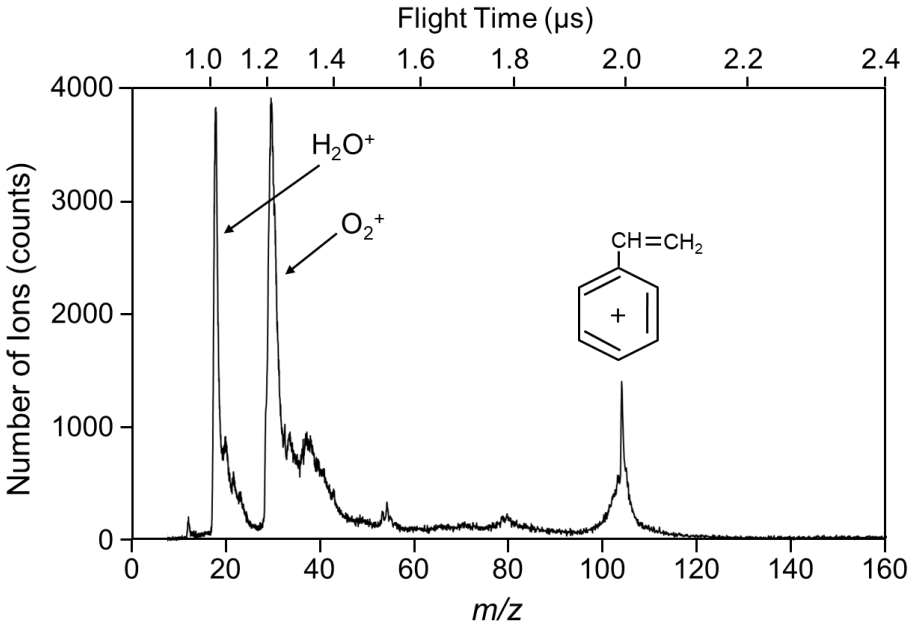

Figure S35. Mass spectrum of styrene prepared using a standard gas generator at 0.1 ppm and diluted with the air (mixing ratio, unknown). Laser power, 200 mW; accumulation time, 0.5 s. Voltage of the electrode; repeller, +0.35 kV; extraction, -1.01 kV; flight tube, -1.0 kV. The signals assigned to H_2O and O_2 appeared from the constituents in the air. A linear analytical curve was constructed in the range of 0-0.5 ppm.

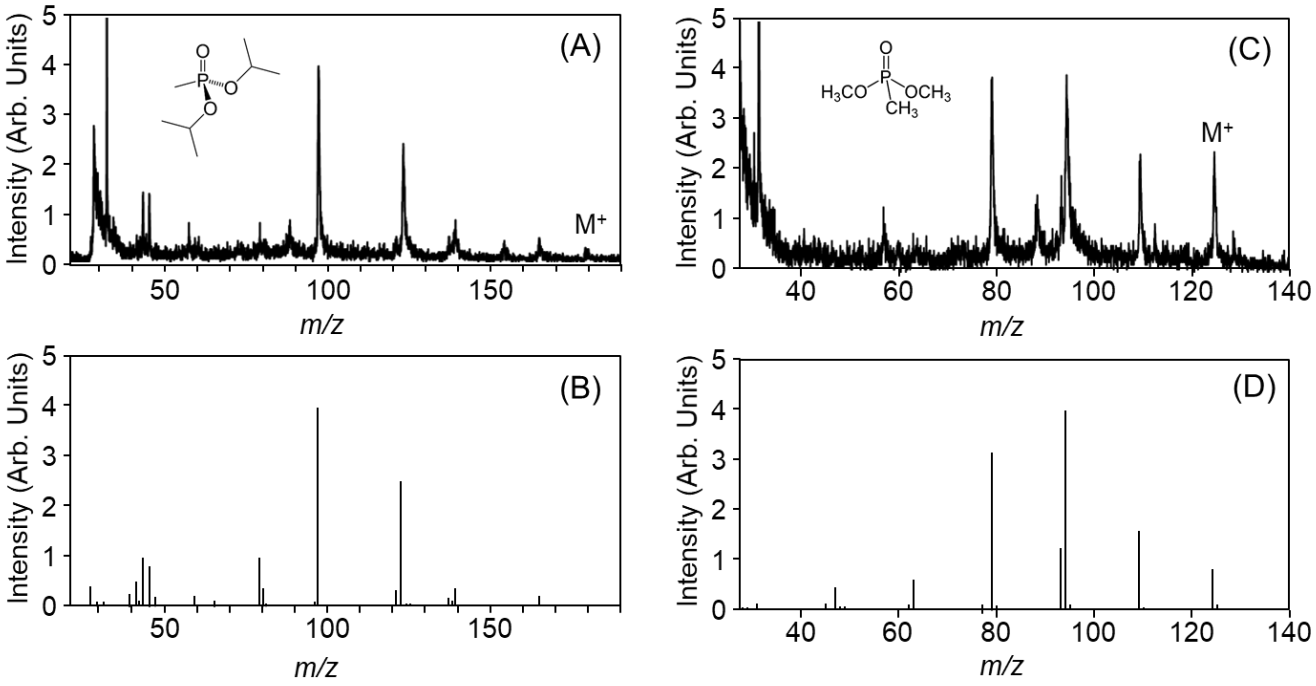

Figure S36. Mass spectra of (A) (B) DIMP (C) (D) DMMP. (A) (C) fs-LIMS (B) (D) EIMS. Laser power, 100 mW; accumulation time, 1 s. The mass spectra measured by EIMS were cited from the NIST database.

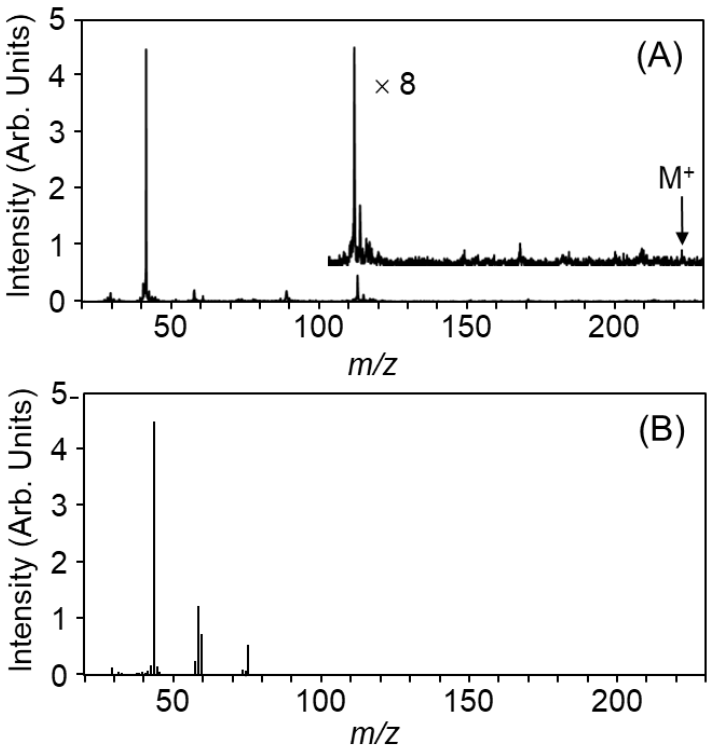

Figure S37. Mass spectra of TATP. (A) fs-LIMS (B) EIMS cited from the NIST database. Laser power, 100 mW; accumulation time, 1 s.

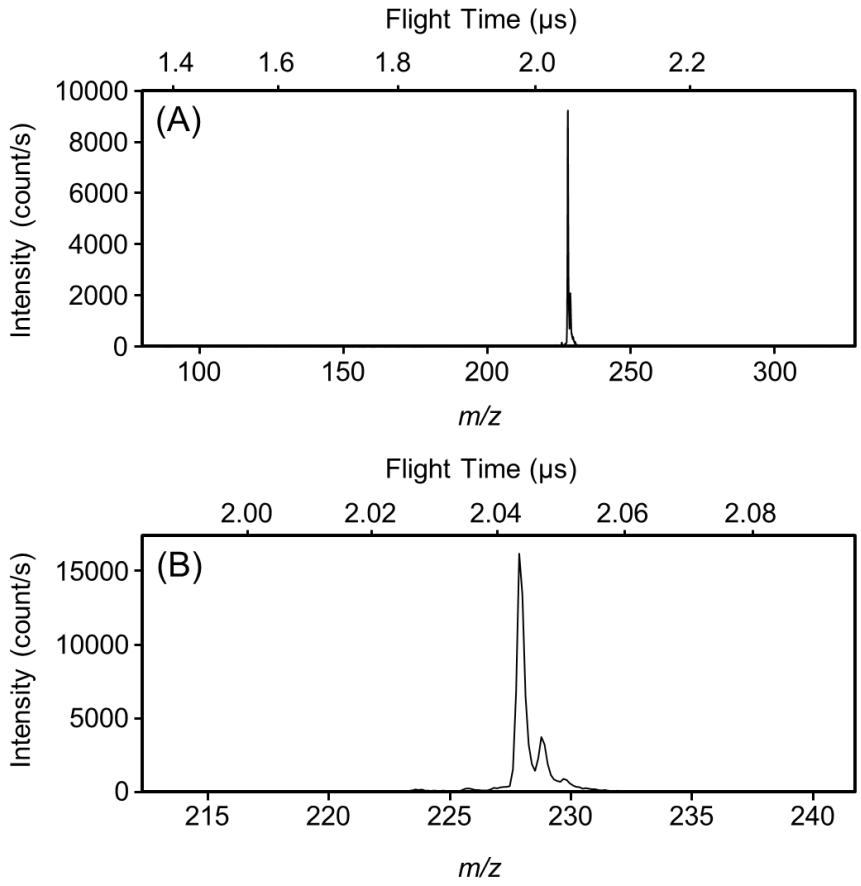

Figure S38. Mass spectra extracted from the two-dimensional display at the retention time, where benzo[a]anthracene appeared. (A) total view (B) expanded view.

Table S1. Photon energy of harmonic emissions and their possible applications.

	Photon Number	Photon Energy (eV)	Combination of Two Photons	Applications	Ionization Process
1	5	5.98	FHG (4) + F (1)	-	-
2	6	7.18	THG (3) + THG (3)	APAH (6.5-7.2 eV)	3 + 3 (RE2PI)
3	6	7.18	FHG (4) + SHG (2)	DMA (7.13 eV)	4 + 2 (RE2PI)
4	6	7.18	FIHG (5) + F (1)	APAH (6.5-7.2 eV)	5 + 1 (RE2PI)
5	7	8.40	FHG (4) + THG (3)	NPAH (7.4-7.5 eV)	3 + 4 (RE2PI)
6	7	8.40	FIHG (5) + SHG (2)	NPAH (7.4-7.5 eV)	5 + 2 (RE2PI)
7	8	9.64	FHG (4) + FHG (4)	aromatic	4 + 4 (RE2PI)
8	8	9.64	FIHG (5) + THG (3)	aromatic/aliphatic	5 + 3 (RE2PI)
9	9	10.96	FIHG (5) + FHG (4)	acetone (9.7 eV), etc.	5 + 4 (RE2PI)
10	10	12.00	FIHG (5) + FIHG (5)	aliphatic	5 + 5 (NR2PI)

F, fundamental; SHG, second harmonic; THG, third harmonic: FHG, fourth harmonic; FIHG, fifth harmonic. APAH, amino polycyclic aromatic hydrocarbon; DMA, dimethylamine; NPAH, nitro polycyclic aromatic hydrocarbon; aromatic, aromatic hydrocarbon; aliphatic, aliphatic hydrocarbon.

Table S2. Ionization energies of compounds related to the combustion of polystyrene.

Compound	Molecular weight	Ionization energy (eV), observed	Ionization energy (eV), calculated	Ionization process
propane	44	10.94 ± 0.05 (113.3 nm)	11.5967 (106.91 nm)	NR3PI
butane	58	10.53 ± 0.02 (117.7 nm)	11.3041 (109.68 nm)	NR3PI
benzene	78	9.24378 ± 0.00007 (134.13 nm)	9.2364 (134.24nm)	RE2PI
toluene	92	8.828 ± 0.001 (140.450 nm)	8.7848 (141.14 nm)	RE2PI
styrene	104	8.464 ± 0.001 (146.49 nm)	8.3455 (148.57 nm)	RE2PI
α-methylstyrene	118	8.3 ± 0.1 (149 nm)	8.3163 (149.09 nm)	RE2PI
1,3-diphenylbutane	210	-	8.5402 (145.18 nm)	RE2PI
2,4-diphenyl-2-pentene	222	-	7.8824 (157.29 nm)	RE2PI
2,4-diphenyl-4-methyl-2(E)-pentene	236	-	7.8630 (157.68 nm)	RE2PI
1,3,5-triphenylhexane	314	-	8.4654 (146.46 nm)	RE2PI
CO_2	44	13.777 ± 0.001 (89.99 nm)		NR3PI
O_2	32	12.0697 ± 0.0002 (102.73 nm)	-	NR3PI
N_2	28	15.581 ± 0.008 (79.577 nm)	-	NR4PI
H_2O	18	12.621 ± 0.002 (98.240 nm)	-	NR3PI

Table S3. Ionization energies of compounds related to combustion of polycarbonate.

Compound	Molecular weight	Ionization energy (eV), observed	Ionization energy (eV), calculated	Ionization process
phenol	94	8.49 ± 0.02 (146.0 nm)	8.4457 (146.80 nm)	RE2PI
p-cresol	108	8.34 ± 0.03 (148.7 nm)	8.1020 (153.03 nm)	RE2PI
styrene	104	8.464 ± 0.001 (146.49 nm)	8.3455 (148.57 nm)	RE2PI
α-methylstyrene	118	8.3 ± 0.1 (149 nm)	8.3163 (149.09 nm)	RE2PI
p-vinylphenol	120	-	7.8434 (158.08 nm)	RE2PI
4-isopropylphenol	136	-	8.0365 (154.28 nm)	RE2PI
dimethyldiphenyl-methane	196	-	7.8997 (156.95 nm)	RE2PI
4-hydroxydiphenyl-dimethylmethane	212	-	8.5402 (145.18 nm)	RE2PI
bisphenol A	228	-	7.7640 (320.13 nm)	RE2PI
O_2	32	12.0697 ± 0.0002 (102.73 nm)	-	NR3PI
N_2	28	15.581 ± 0.008 (79.577 nm)	-	NR4PI
H_2O	18	12.621 ± 0.002 (98.240 nm)	-	NR3PI

References

(S1) Imasaka, T.; Hozumi, M.; Ishibashi, N. Supersonic jet spectrometry of chemical species resulting from thermal decomposition of polystyrene and polycarbonate. *Anal. Chem.* **1992**, *64*, 2206-2209.

(S2) Müller, M.; Klenke, A.; Gottschall, T.; Klas, R.; Rothhardt, C.; Demmler, S.; Rothhardt, J.; Limpert, J.; Tünnermann A. High-average-power femtosecond laser at 258 nm. *Opt. Lett.* **2017**, *42*, 2826-2830.